J. Fluid Mech. (1984), *vol.* 142, *pp.* 343–362
Printed in Great Britain

The structures and energetics of fully nonlinear symmetric baroclinic waves

By TIMOTHY L. MILLER

Space Science Laboratory, NASA Marshall Space Flight Center, Huntsville, Alabama 35812

(Received 13 July 1983 and in revised form 6 January 1984)

A finite-difference Navier–Stokes model has been used to study rotating baroclinic flow for Richardson number $\lesssim 1$, assuming no variations except in the vertical plane wholly containing the density-gradient vector. A section of a horizontally infinite channel has been studied, assuming periodic boundary conditions at the vertical computational boundaries and no-slip conducting horizontal boundaries. Two configurations were studied, both of which have an analytic basic solution with no horizontal variations in the velocities or density gradients. Symmetric baroclinic waves developed in the flows, as long as the Richardson number was not too large and the thermal Rossby number was large enough (for fixed diffusion parameters), consistent with linear theory. The structures and energetics of the fully developed waves were found to be especially dependent upon the Prandtl number Pr. Potential energy was the ultimate wave-energy source in all cases, and the average zonal flow was never much affected by the waves. For $Pr > 1$ the conversion from potential energy to wave kinetic energy was direct, via temperature and vertical-motion correlation. For $Pr < 1$ the conversion was from potential energy, to average kinetic energy by virtue of an induced meridional flow, to wave kinetic energy. For $Pr = 1$ the energy conversion was by either or both of the above, depending upon the other parameters.

1. Introduction

In the mid-1960s symmetric baroclinic instability (hereafter SBI) received a revival in interest, with work by Ooyama (1966), Stone (1966, 1970, 1972), McIntyre (1970*a*), Yanai & Tokioka (1969), Tokioka (1970) and others. The physical mechanism for the instability is simply explained as a combined effect of buoyancy and inertial restoring forces (see Hoskins 1978). This is illustrated in figure 1, which is drawn in a vertical plane wholly containing the basic density (or temperature) gradient (the 'meridional' plane). For simplicity a zonal flow in thermal wind balance with a constant temperature gradient is considered. For Richardson number Ri between 0 and 1 the flow is stable in both the convective and inertial sense, but may be unstable when the two restoring forces act together. The instabilities consist of meridional motions at angles intermediate to those of angular momentum M and temperature T contours, with deviation temperature and zonal momentum structures compatible with those motions. If diffusion is present the two restoring forces are damped; if the Prandtl number (viscosity divided by thermal diffusivity) differs from unity the dampings of the two forces are unequal. McIntyre (1970*a*) has shown that in this case instability can occur for $Ri > 1$ (all boundary effects ignored).

The energy-release mechanism for SBI can be either buoyancy or inertial or a combination of the two (Stone 1972; Tokioka 1970). This appears to be a source of

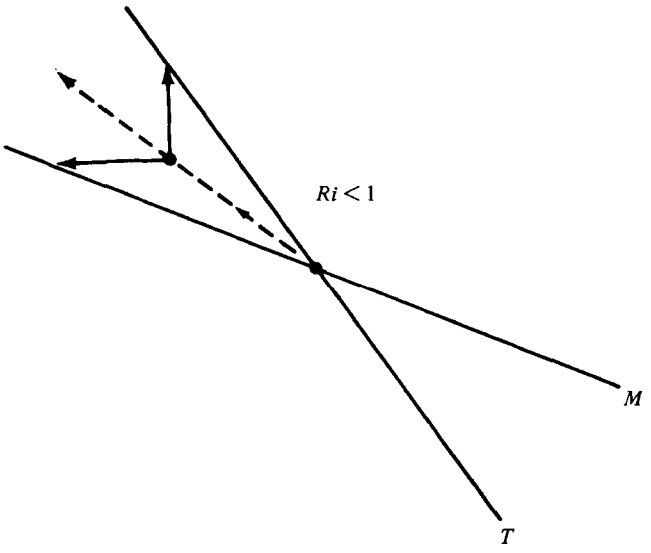

FIGURE 1. For Richardson number Ri less than 1 (i.e. isotherms more vertical than angular momentum surfaces) a fluid particle displaced at an angle intermediate to those of temperature and angular momentum surfaces will feel a vertical buoyancy restoring force and a horizontal inertial restoring force, resulting in a net force *away* from the initial position.

confusion, since previous authors (e.g. Emanuel 1979); Weber 1980; Busse & Chen 1981) have stated that the inertial mechanism is the source. This is true for the fastest-growing inviscid mode, which has zero wavelength (Stone 1972), and for Emanuel's viscous hydrostatic waves for the particular cases he considered. However, the energy source may be expected, in general, to be dependent upon the particular combination of parameters. In particular, one would expect a strong Prandtl-number dependence, since one of either the inertial or buoyancy forces can become dominant for $Pr \neq 1$. This point has not been ellucidated in previous works, although from the work of McIntyre it may be seen that the angles of the meridional motion for cases of $Ri > 1$ are such that heat and angular momentum are transported upward for $Pr > 1$ and downward for $Pr < 1$. (That is, the motions are more to the horizontal in the former case and more to the vertical in the latter.)

Unlike the conventional, three-dimensional baroclinic instability associated with large Richardson numbers, SBI has not been well observed, either in the laboratory or in the atmosphere. Bennetts & Hoskins (1979), Weber (1980) and Emanuel (1979, 1982) have discussed the possible importance of SBI in organizing mesoscale systems in the atmosphere, although there have been no reports of detailed observations of the phenomenon. Calman (1977) suggests SBI as an explanation of some oceanic phenomena. In thermally driven laboratory experiments, Stone *et al.* (1969) and Hadlock, Na & Stone (1972) claimed to have found symmetric baroclinic instability. In these experiments the horizontal temperature gradient was supplied by upper and lower conducting boundaries, the sidewalls being insulators. In this manner the interior Richardson number was constrained to be small, whereas in the side-heated annulus (e.g. Fowlis & Hide 1965) meridional overturning results in the interior Richardson number being large. The results of the experiments by Stone *et al.* and Hadlock *et al.* were, however, inconclusive, primarily because of the lack of detailed

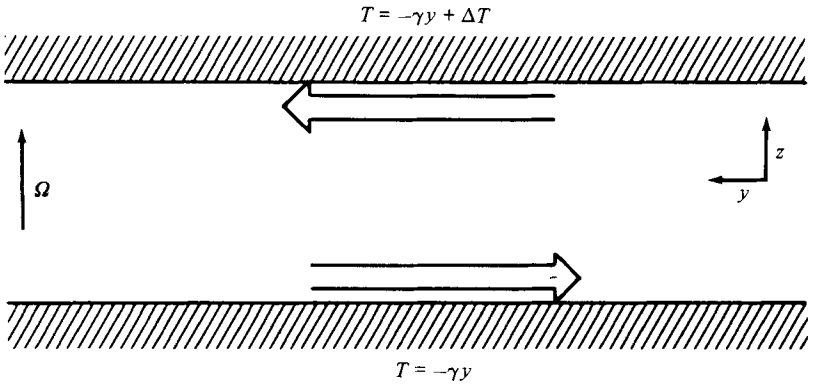

FIGURE 2. Schematic diagram of the rotating channel, with an imposed temperature gradient on the horizontal surfaces. Arrows indicate direction of the Hadley cell.

measurements or other definitive observations. In numerical, studies Quon (1980, 1981) found that Bénard-type symmetric instability of the horizontal boundary layers in these experiments were likely to prevent the formation of orderly symmetric baroclinic cells.

In a mechanically driven experiment Calman (1977) found an apparently symmetric instability for effectively a large Prandtl number. However, Calman reported that the effect of the waves upon the average potential energy (density profile with height) was insignificant, and that the effect on average zonal velocity was large, which is at variance with the results of the present study for large Prandtl number. Indeed, if the diffusion of density (salt in Calman's case) is very small, then one would expect that the advection by the meridional motions could carry the density variations with the flow (unless all motion is within a region of constant density) and thus affect the mean potential energy. Calman offered no theoretical explanation for his mean-transport observations.

Williams (1968, 1970) and McIntyre (1970*b*) point to symmetric baroclinic instabilities in calculations of flow in a side-heated annulus with free surfaces everywhere except the bottom (not, of course, physically realizable). The evidence supporting the presence of SBI was particularly strong for $Pr = 7$. When no-slip sidewalls are assumed in the calculations, the meridional heat transport by the viscous sidewall layers and the constraint upon the angular momentum contours result in a larger Ri, suppressing SBI.

Despite the scarcity of evidence that SBI may physically exist, it has been extensively theoretically studied – as we have already mentioned. The more recent works have included full viscous effects on flow confined between infinite horizontal boundaries. The study by Antar & Fowlis (1982) considers the stability of a rotating Hadley cell in an infinite channel with a constant horizontal temperature gradient imposed upon the upper and lower boundaries (figure 2). In this case there exists a solution to the full (Boussinesq) Navier–Stokes equations (with centrifugal force neglected) in which velocities and thermal gradients are independent of y. The known existence of a basic state and the fact that it is an approximation to the experiments of Stone *et al.* and Hadlock *et al.* makes this configuration appear to be attractive for systematic study. Antar & Fowlis calculated SBI growth rates and constructed critical curves in parameter space for varying Prandtl number, thermal Rossby number, Ekman number and vertical temperature difference. The approximate

Richardson number at mid-depth is a simple function of these. Their results for very small Ekman number agreed well with those of McIntyre (1970*a*) when the Prandtl number was not small; agreement was fair for small Prandtl number. This study did not investigate any finite-amplitude effects, nor did they report on energy conversions.

Another, simpler, basic state that is a solution to the full equations was used in the other referenced works. In this case, the upper and lower boundaries move with the zonal flow, and therefore there is no basic meridional flow (i.e. no boundary layers) in the basic state. As we shall see, this configuration (hereinafter the 'Eady' basic state) is more generally amenable to the type of study undertaken here.

Walton (1975) has performed a viscous hydrostatic study of SBI, including effects of upper and lower boundaries in the stability problem and also examining weak nonlinearity in the flow. Although Walton examined the horizontal angular momentum wave flux, he did not examine the energetics, and in particular the dependence of the energetics on Prandtl number – perhaps the most interesting result of the present study. Weber's (1980) study was a linear non-hydrostatic study of the same configuration as Walton, and pointed out the dependence of the critical Richardson number upon the Rossby, Prandtl and Ekman numbers. He did not calculate eigenfunctions or their energetics.

The existence of known basic states (solutions to the full equations) puts the previously described baroclinic configurations on a par with the Bénard-convection problem in opportunity for the numerical study of fully nonlinear evolution of two-dimensional instabilities. In this study we have used a finite-difference Navier–Stokes model to calculate flows in a section of a horizontally 'infinite' domain, assuming periodicity at the endwalls of the section. We have focused our efforts upon the structures and energetics of fully developed steady waves, and upon the dependence of these upon the Prandtl, Rossby, Ekman and Richardson numbers.

2. Equations and models

2.1. *Basic equations*

We consider a channel of effectively infinite horizontal extent, rotating about a vertical axis far from the region of interest with rate Ω. Gravity g is downward, and centrifugal buoyancy effects are neglected. The upper and lower boundaries are rigid surfaces, separated by a distance D. The fluid's thermal expansivity, viscosity and thermal diffusivity are denoted by α, ν and κ respectively. Upon the horizontal plates is imposed a constant temperature gradient of amplitude γ.

We take as our coordinate system the Cartesian (x, y, z) where z increases upward and y increases in the direction of the horizontal projection of $-\nabla T$. We may think of the direction of increasing y as 'northward' and the direction of increasing x as 'eastward'. Distance, time, velocity, temperature and pressure are non-dimensionalized by the quantities D, Ω^{-1}, $g\alpha D\gamma/\Omega$, γD and $g\alpha\rho_0\gamma D^2$ following Antar & Fowlis (1982) (ρ_0 is a reference density). The Boussinesq system of equations governing the flow assuming $\partial/\partial x \equiv 0$ are

$$\frac{\partial u}{\partial t} + Ro\left(v\frac{\partial u}{\partial y} + w\frac{\partial u}{\partial z}\right) - 2v = E\left(\frac{\partial^2 u}{\partial y^2} + \frac{\partial^2 u}{\partial z^2}\right), \tag{2.1}$$

$$\frac{\partial v}{\partial t} + Ro\left(v\frac{\partial v}{\partial y} + w\frac{\partial v}{\partial z}\right) + 2u = -\frac{\partial P}{\partial y} + E\left(\frac{\partial^2 v}{\partial y^2} + \frac{\partial^2 v}{\partial z^2}\right), \tag{2.2}$$

$$\frac{\partial w}{\partial t}+Ro\left(v\frac{\partial w}{\partial y}+w\frac{\partial w}{\partial z}\right)=T-\frac{\partial P}{\partial z}+E\left(\frac{\partial^2 w}{\partial y^2}+\frac{\partial^2 w}{\partial z^2}\right), \tag{2.3}$$

$$\frac{\partial T}{\partial t}+Ro\left(v\frac{\partial T}{\partial y}+w\frac{\partial T}{\partial z}\right)=\frac{E}{Pr}\left(\frac{\partial^2 T}{\partial y^2}+\frac{\partial^2 T}{\partial z^2}\right), \tag{2.4}$$

$$\frac{\partial v}{\partial y}+\frac{\partial w}{\partial z}=0, \tag{2.5}$$

where
$$Ro=\frac{g\alpha\gamma}{\Omega^2},\quad E=\frac{\nu}{\Omega D^2},\quad Pr=\frac{\nu}{\kappa}, \tag{2.6}$$

are the Rossby, Ekman and Prandtl numbers. Here T is the temperature deviation from a reference value and P is the pressure deviation from the hydrostatic at the reference temperature. The velocity components u, v and w correspond to the coordinates x, y and z.

When the rigid horizontal plates are corotating at rate Ω the boundary conditions are

$$\left.\begin{aligned} u=v=w&=0,\\ T&=\pm\tfrac{1}{2}\Delta T-y\end{aligned}\right\} \tag{2.7}$$

at $z=\pm\frac{1}{2}$, where ΔT is the dimensionless temperature difference between the top and bottom plates for fixed y.

There exists a solution to (2.1)–(2.7) in which velocities and temperature gradients are independent of y:

$$\left.\begin{aligned} U(z)&=-\tfrac{1}{8}f(z)+\tfrac{1}{2}z,\\ V(z)&=-\tfrac{1}{8}g(z),\\ T(y,z)&=-y+z\Delta T+\tfrac{1}{8}Ro\,Pr(2z-\tfrac{1}{2}f(z)),\\ W&\equiv 0,\end{aligned}\right\} \tag{2.8}$$

where

$$\left.\begin{aligned} f(z)&=[\cosh R(z+\tfrac{1}{2})\cos R(z-\tfrac{1}{2})\\ &\quad-\cosh R(z-\tfrac{1}{2})\cos R(z+\tfrac{1}{2})]/h(R),\\ g(z)&=[\sinh R(z+\tfrac{1}{2})\sin R(z-\tfrac{1}{2})\\ &\quad-\sinh R(z-\tfrac{1}{2})\sin R(z+\tfrac{1}{2})]/h(R),\\ h(R)&=\sinh^2\tfrac{1}{2}R+\sin^2\tfrac{1}{2}R,\\ R&=E^{-\frac{1}{4}}.\end{aligned}\right\} \tag{2.9}$$

This solution is given in Antar & Fowlis (1982). The basic-state velocity components and temperature profile for a particular case may be seen in figure 4. A meridional flow in Ekman layers (i.e. the Hadley cell) results in significant thermal advection (for Pr not too small). There exist thermal boundary layers in which $\partial T/\partial z<0$, and in which Bénard-like convection can occur, depending of course upon the parameters. A local Rayleigh number may be defined as

$$Ra_{\mathrm{B}}=\frac{-g\alpha\Delta T_{\mathrm{B}}D_{\mathrm{B}}^3}{\nu\kappa}, \tag{2.10}$$

where ΔT_{B} is the negative dimensional temperature difference in the boundary layers, and D_{B} is the depth of those layers. We may expect boundary-layer instability if Ra_{B}

becomes much larger than 10^3; the exact critical Ra_B is presumably a function of the other parameters and is not determined in this investigation.

The Richardson number

$$Ri = g\alpha \frac{\partial T^*}{\partial z^*} \Big/ \left(\frac{\partial u^*}{\partial z^*}\right)^2,$$

where the asterisk denotes dimensional quantities. Ri is a function of space, but at the midpoint in the Hadley-cell model

$$Ri \approx Pr + \frac{4\Delta T}{Ro}. \tag{2.11}$$

In the configuration with moving boundaries the boundary condition on the dimensionless u becomes

$$u = \pm\tfrac{1}{4} \quad \text{at} \quad z = \pm\tfrac{1}{2}, \tag{2.12}$$

and all other boundary conditions are the same as (2.7). In this case the basic state is simply

$$\left.\begin{aligned} V = W &\equiv 0, \\ U &= \tfrac{1}{2}z, \\ T &= -y + z\,\Delta T. \end{aligned}\right\} \tag{2.13}$$

The Richardson number is constant in space and is $4\,\Delta T/Ro$. In the Eady-state model, the (possibly unstable) boundary layers in the basic state do not exist. Of course, there will exist boundary layers in the waves, and conceivably these could become unstable if the waves become strong enough.

2.2. *Numerical technique*

A computer code was adapted from that of Miller & Gall (1983*a*), in which the basic equations in spherical coordinates are solved by standard time-marching finite-difference methods. All curvature terms were removed, and the code used in the present study is in Cartesian geometry. The horizontal extent of the integration domain is a finite distance L, and periodic boundary conditions on u, v, w, and ∇T are assumed at the endwalls. The grid is regular in the horizontal, and it is stretched in the vertical to increase resolution near the boundaries. The stretching function used here is

$$\left.\begin{aligned} \Delta z(k) &= \{\tfrac{1}{2}[1 - \cos 2\pi z_s\}^\beta / \Gamma + \delta, \\ z_s &= \frac{k-1}{K-1}, \\ \Gamma &= \sum_k \{\tfrac{1}{2}[1 - \cos 2\pi z_s]\}^\beta, \end{aligned}\right\} \tag{2.14}$$

where k is the vertical index and δ and β are grid parameters, along with the number of intervals in the horizontal (J) and vertical (K) and the length L. Larger δ gives less stretching; the parameter β controls where the fastest stretching occurs. These parameters are given in tables 1 and 2 which are summaries of calculations performed. Obviously, care must be taken to choose all of these parameters appropriately. For example, L must be large enough to accommodate the most-favoured wavelengths for a particular case, but it cannot be so large (for fixed J) that important (short) wavelengths are poorly resolved. The choice of L was initially guided by the results of Weber (1980) and Antar & Fowlis (1982). In all cases (unless Ri/Ri_c was fairly small) it was found that the dominant wavelength here was somewhat longer than

the critical wavelength from Wever (1980). For those cases that are studied here in some detail (cases B1, B2, B3), that L which gave maximum total kinetic energy density was found to within 10%.

In all cases reported here the initial condition for the integration was the analytic basic state. In the Hadley-cell model computer round-off error was sufficient to perturb the basic state and to initiate wave growth. In the Eady-state model, where there is no meridional flow in the basic state, a small random meridional flow and temperature perturbation were used to initiate instabilities.

2.3. *Energy conversions*

All components u, v, w and T may be partitioned into 'horizontal-average' and 'deviation' values:

$$u(y,z,t) = \bar{u}(z,t)+u'(y,z,t),$$
$$v(y,z,t) = \bar{v}(z,t)+v'(y,z,t),$$
$$w(y,z,t) = 0+w'(y,z,t),$$
$$T(y,z,t) = -y+\bar{T}(z,t)+T'(y,z,t),$$

where the horizontal averages of all deviation (primed) quantities are zero. Kinetic- and potential-energy equations can be derived from (2.1)–(2.4) in the usual manner:

$$\frac{\partial\langle \mathrm{KE}\rangle}{\partial t} = \langle w'T'\rangle+\langle \bar{v}z\rangle+\langle F\rangle$$
$$= \langle E_1\rangle+\langle E_4\rangle+\langle F\rangle, \tag{2.15}$$

$$\frac{\partial\langle \mathrm{KE}'\rangle}{\partial t^*} = \langle w'T'\rangle - R_0\left\langle w'u'\frac{\partial\bar{u}}{\partial z}\right\rangle - R_0\left\langle w'v'\frac{\partial\bar{v}}{\partial z}\right\rangle+\langle F'\rangle$$
$$= \langle E_1\rangle+\langle E_2\rangle+\langle E_3\rangle+\langle F'\rangle \tag{2.16}$$

$$\frac{\partial\langle \overline{\mathrm{KE}}\rangle}{\partial t^*} = \langle E_4\rangle-\langle E_2\rangle-\langle E_3\rangle-\langle \bar{F}\rangle, \tag{2.17}$$

$$\frac{\partial\langle \mathrm{PE}\rangle}{\partial t^*} = -\langle w'T'\rangle-\langle \bar{v}z\rangle+\langle D\rangle$$
$$= -\langle E_1\rangle-\langle E_4\rangle+\langle D\rangle, \tag{2.18}$$

where

$$\mathrm{KE} = \tfrac{1}{2}(u^2+v^2+w^2), \tag{2.19}$$
$$\mathrm{KE}' = \tfrac{1}{2}(u'^2+v'^2+w'^2), \tag{2.20}$$
$$\overline{\mathrm{KE}} = \mathrm{KE}-\mathrm{KE}', \tag{2.21}$$
$$\mathrm{PE} = -zT/Ro. \tag{2.22}$$

The angular brackets $\langle\ \rangle$ refer to volume integration throughout space, and $\langle F\rangle$ and $\langle D\rangle$ refer to viscous and conductive dissipation.

An important consideration for the purposes here is the signs and the relative sizes of the individual terms on the right-hand side of (2.16). If the first term is positive and dominates, then the extraction of energy for the waves is primarily of a convective nature. That is, the wave kinetic energy is obtained directly from the flow's potential energy. If the second or third terms are positive and dominant, the wave energy is obtained from the kinetic energy of the horizontal average state. The term $\langle E_4\rangle$ represents $\mathrm{PE}\leftrightarrow\mathrm{KE}$ conversion due to heat being advected into and out of the finite section of the channel. In the Eady-state model this term has entirely

nonlinear origins, since there is no $\bar{v}$ in the basic state. In the Hadley-cell model this conversion is present in the basic state, due to the boundary layers, and is balanced by conduction through the upper and lower boundaries. Of interest here is the difference between the value of this term in the analytic basic state and its value after waves have developed.

2.4. *Angular momentum*

In the infinite-channel model, angular momentum is not strictly defined, since the radius outward from the axis of rotation is not defined. A quantity M, whose derivatives are defined below, can be easily shown to be the quantity that is analogous to angular momentum in terms of inertial stability (see Hoskins 1978):

$$\left.\begin{aligned} \frac{\partial M}{\partial y} &= \frac{\partial u}{\partial y} - 2, \\ \frac{\partial M}{\partial z} &= \frac{\partial u}{\partial z}. \end{aligned}\right\} \tag{2.23}$$

Thus $M = u - 2y$, where y is measured from an arbitrary origin. Note that here y increases *towards* the axis of rotation and that a positive $\partial M/\partial y$ is an inertially unstable situation.

3. Results and discussion

The computer code is based upon the dimensional equations, and results are shown in c.g.s. units. In all cases shown here Ω, γ and D are 1 in c.g.s. units. Ro is varied by changing $g\alpha$, Ri is varied by changing either Ro or ΔT in the Eady-state model and either Ro, ΔT or Pr in the Hadley-cell model. Note that a fixed ΔT in the former model implies that the slope of the basic state isotherms throughout the fluid is fixed. Fixing ΔT in the Hadley-cell model does not imply this: As Ro or Pr are varied the boundary-layer advection changes, and the slope of the interior isotherm changes. Note, however, that if Pr and ΔT are changed while fixing Ro and Ri, the slope of the interior isotherms remains constant.

The results shown here, unless noted otherwise, are for integrations which have been conducted until the waves were fully developed and the rates of change of the integrated energy components were small. For example, case A1 was integrated twice as long as shown in figure 5. The stream function (ψ) shown in the plots is defined by $\partial\psi/\partial z = -v$, $\partial\psi/\partial y = w$.

3.1. *Corotating boundaries*

This is the model studied by Antar & Fowlis (1982). As mentioned previously, we may expect to run into trouble seeking SBI owing to convective instability in the boundary layers, and indeed this was a complication. The results of calculations are summarized in table 1. There were cases where boundary-layer convection occurred as the primary instability, and two cases where it occurred along with SBI or may have been a secondary instability.

An example of steady well-developed SBI waves for $Pr = 1$ is shown in figure 3 (case A1). The meridional motions consist of cells (imposed upon the basic Ekman flow) oriented at midlevel at an angle slightly to the horizontal of the basic isotherms. The cells are rather symmetric; i.e. the clockwise ones are of about the same size and shape as the counterclockwise ones. On the average, heat is transported upward, and thus the convective energy-conversion term $\langle E_2 \rangle$ in (2.16) is positive. The term $\langle E_2 \rangle$

Case	*Ro*	*Ri*	*E*	*Pr*	*L*	Results
A1	3.75	0.68	0.001	1.00	2.4	Steady symmetric baroclinic waves
A2	5.0	0.68	0.001	1.0	2.4	Symmetric baroclinic waves and boundary-layer instability; persistent unsteadiness
A3	3.75	0.68	0.001414	2.0	2.4	Concurrent boundary-layer convection and SBI; persistent unsteadiness
A4	3.75	0.68	0.000707	0.5	2.4	Steady symmetric baroclinic waves
A5	5.0	0.84	0.001	1.0	2.0	Very weak SBI
A6	2.5	0.68	0.001	1.0	2.0	Weak SBI
A7	10	0.92	0.001	1.0	2.0	Boundary-layer convection, followed by 'chaotic' flow throughout

TABLE 1. Cases computed for the Hadley-cell model. The numerical parameters were $J = 21$, $K = 23$, $\beta = 1.5$, $\delta = 0.11$ for all cases.

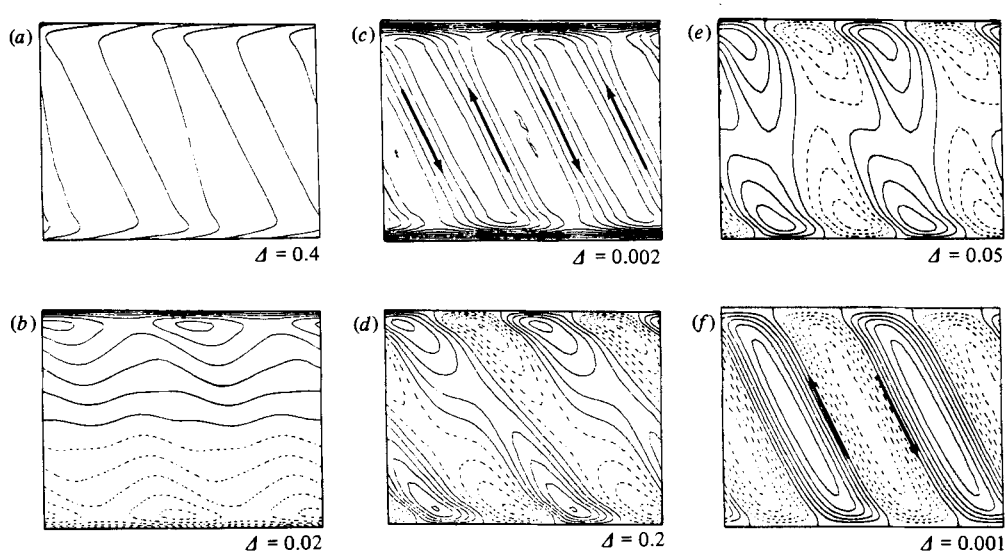

FIGURE 3. Results of calculations for case A1: (*a*) temperature; (*b*) zonal velocity; (*c*) total stream function; (*d*) deviation temperature; (*e*) deviation zonal velocity u; (*f*) deviation stream function. The coordinate z increases upward, y increases to the left. Dashed contours indicate negative values, Δ is the contour interval. See table 1 for true length/height aspect ratio.

in (2.16) is also positive, but much smaller. The magnitude of $\langle E_3 \rangle$ is much smaller than the other energy conversions in this and all other cases in this study; $\langle E_4 \rangle$ (with the basic state v subtracted from $\bar{v}$) is positive and slightly larger than $\langle E_2 \rangle$. (The numbers for $\langle E_1 \rangle$, $\langle E_2 \rangle$ and $\langle E_4 \rangle$ are similar to those of case B1, table 3.) In plots of the average $\bar{u}$, $\bar{v}$ and $\bar{T}$ versus the analytic basic state (figure 4) we see that temperature is significantly affected, reflecting the lowering of the potential energy

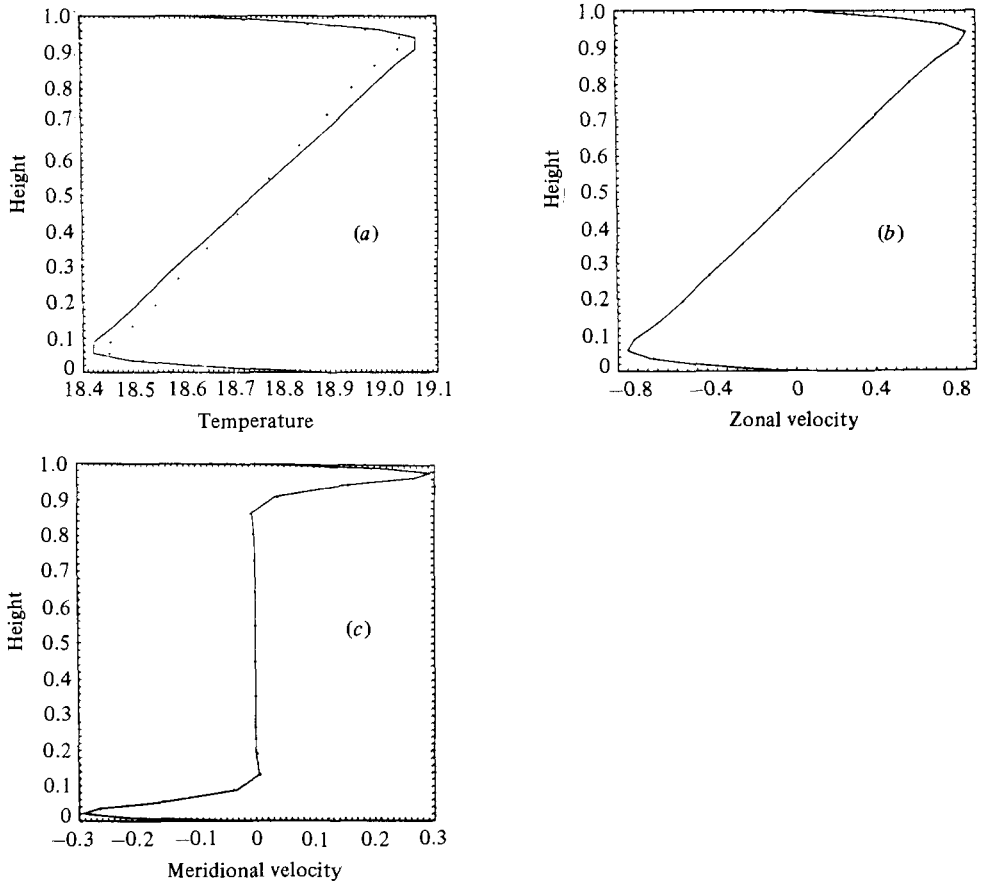

FIGURE 4. Analytic basic state (points) and average values after waves were fully developed (solid curve) for case A1.

by both $\langle E_1 \rangle$ and $\langle E_4 \rangle$. The meridional component $\bar{v}$ is slightly increased, as the waves induce an additional thermally direct meridional circulation. The zonal component $\bar{u}$ is hardly affected at all, although $\langle E_2 \rangle$ is non-zero, indicative of the compensating effect of the increase in $\bar{v}$, which tends to increase $\bar{u}$ via Coriolis deflection. It is noted that most of the contribution to $\langle E_2 \rangle$ is in and near the boundary layers, which is also where the increase in $\bar{v}$ is located.

From the plots of the deviations u' and v', it may be seen that they are positively correlated near the boundaries and negatively correlated in the interior. The amplitudes of u' and v' are largest near the boundary layers. This is also true for the Eady-state model.

The plots of the energy components ($\langle \mathrm{PE} \rangle$, $\langle \mathrm{KE} \rangle$, $\langle \overline{\mathrm{KE}} \rangle$) with time are shown in figure 5. As previously stated, the initial condition was the analytic basic state, and computer round-off error and truncation error due to finite-differencing were allowed to supply the perturbations. The initial small oscillation is due to a computational mode present after the first time step. Both components of KE (KE′ and $\overline{\mathrm{KE}}$) grow at the expense of PE when the wave develops. The waves 'overshoot', and KE decreases after some maximum value, after which an approximate equilibration occurs rather rapidly. (That is, there is not much oscillation, at least

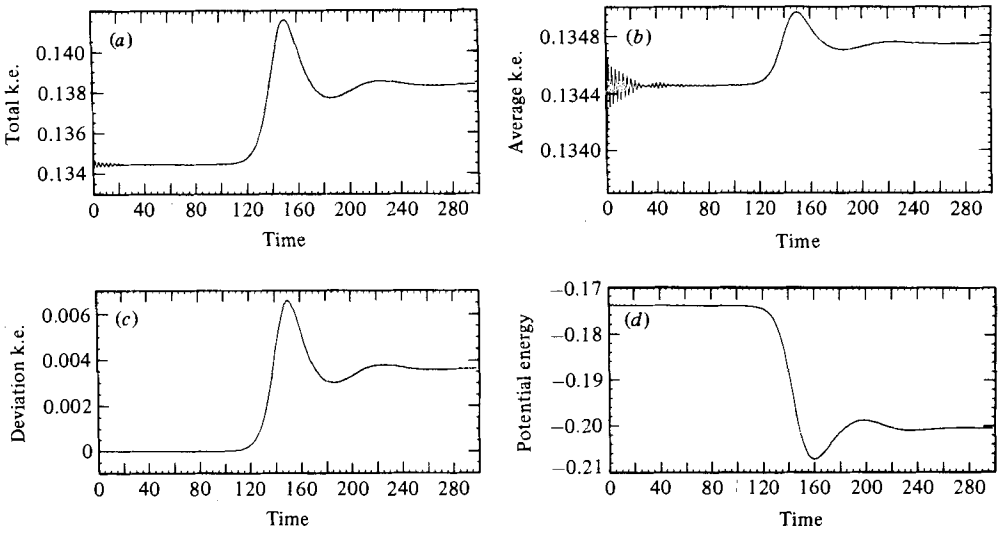

FIGURE 5. Development with time of energy integrals for case A1.

in the same scale as the original overshoot.) The same is true of all cases considered here, except for those noted to be unsteady in tables 1 and 2. For the small-Pr cases the overshoot was much smaller that that of the other cases.

Figure 6 shows a case (for larger $-\Delta T$) where both SBI and convection in the boundary layers are developing (case A2). As integration is continued past the point shown, the convection quickly disturbs the Ekman-layer flow to the point that the convectively stable ($\partial T/\partial z > 0$) temperature profile in the interior gives way to a locally unstable profile in some regions, and an unsteady, 'chaotic' flow, with both SBI and convection, is evident. The detailed study of this evolution is beyond the intent of this work. Other cases were considered where the boundary-layer convection was the primary instability, giving rise to convection throughout, and SBI did not have enough time to develop. This was particularly true for $Pr > 1$. Note that for large Pr the effect of thermal advection is greater and therefore Ra_B increases. To fix Ri and Ro with increasing Pr requires increasing the negative vertical temperature difference $-\Delta T$, increasing the chance for convective instability.

For $Pr = 1$, finding a cut-off of instability as Ri nears 1 from below for a fixed ΔT (reported by Antar & Fowlis 1982) was impossible, because as Ro is increased (in order to increase Ri), Ra_B increases (faster than Ro), and boundary-layer convection sets in (see table 1, case A7). Clearly the stability diagrams in Antar & Fowlis (1982) must be interpreted with care. Convective boundary-layer modes were not considered in their analysis (1983 personal communication).

3.2. *Eady basic state (moving boundaries)*

The cases considered in the 'Eady' configuration are summarized in table 2. More-detailed study was given to this case. The primary goal here is to examine how the structures and energetics of the flows change with varying parameters. Ideally we would like to isolate the effects of varying each parameter individually. However, the critical Richardson number Ri_c is in general a function of the other parameters, and hence, if only one parameter is changed, the strength of the equilibrated flow may be very different. We would prefer that the additional complication of increased

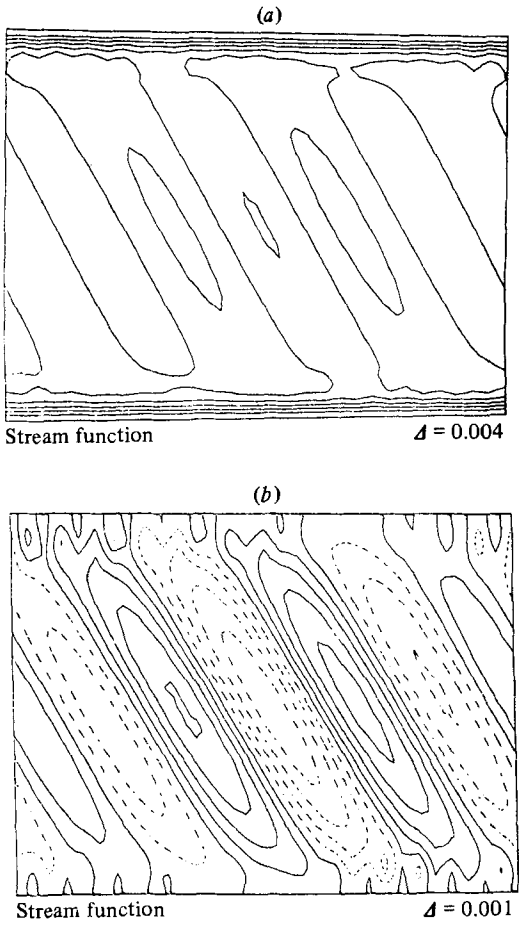

FIGURE 6. Results of calculations for case A2. Contour scheme is as in figure 3. See table 1 for true length/height aspect ratio.

nonlinearity not be present as we compare different cases. Therefore, if a particular set of parameters resulted in waves that were either too weak or too strong to be compared with others, Ri was approximately adjusted by changing ΔT. Weber's (1980) expression (38) was used as an initial guide to Ri_c (see table 2), but note that because of his approximations this expression is not exact.

The cases for $Pr = 1$ and corresponding Ri and Ro were compared with those of §3.1. The energetics and structure of the waves were similar. The discussion there of the case A1 applies here as well. In figure 7 there are presented contour plots for a case (B1) where Ro is somewhat smaller than case A1 in §3.1. These fields will be compared with those for non-unit Prandtl number below. The energy-conversion integrals are given in table 3.

The problems that were encountered with convection in the boundary layers in the basic state of the Hadley-cell model were not, of course, encountered in the Eady-state model. However, the nonlinearity of the flow increased dramatically when Ri/Ri_c is decreased and the waves can become so strong that either one or both of the following can occur: (i) 'fronts' (i.e. strong gradients over a narrow region) can develop such that the grid resolution used here becomes inadequate and (ii) apparently chaotic

Case	*Ro*	*Ri*	Ri_c	*E*	*Pr*	λ_c	*L*	δ	Result
B1	3	0.68	0.83	0.001	1	0.46	2.0	1.0	Moderate, steady SBI; $k = 3$ dominant
B2	3	0.83	1.01	0.001	2	0.56	2.2	1.0	Same as B1
B3	3	0.83	0.78	0.001	0.5	0.42	2.0	1.0	Same as B1
B4	3	0.68	1.40	0.002	4	1.1	3.6	1.0	Highly nonlinear SBI; chaotic behaviour; $k = 4$ dominant
B5	3	0.68	1.27	0.0005	0.25	0.34	2.2	1.0	Same as B4
B6	24.7	0.48	0.56	0.02	1	6.1	20.0	10.0	Same as B1
B7	24.7	0.84	0.94	0.001	1	2.3	9.0	1.0	Same as B1
B8	5	0.16	—	0.02	1	—	6.0	10.0	Moderate, steady SBI; $k = 4$ dominant
B9	7.5	0.68	0.93	0.001	1	0.79	4.0	1.0	Same as B4, but $k = 3$ dominant

TABLE 2. Cases computed for Eady-state model. The numerical parameter β was 1.0, and K was 25 for all cases. J was 31 for cases B4 and B5, and was 49 for all others.

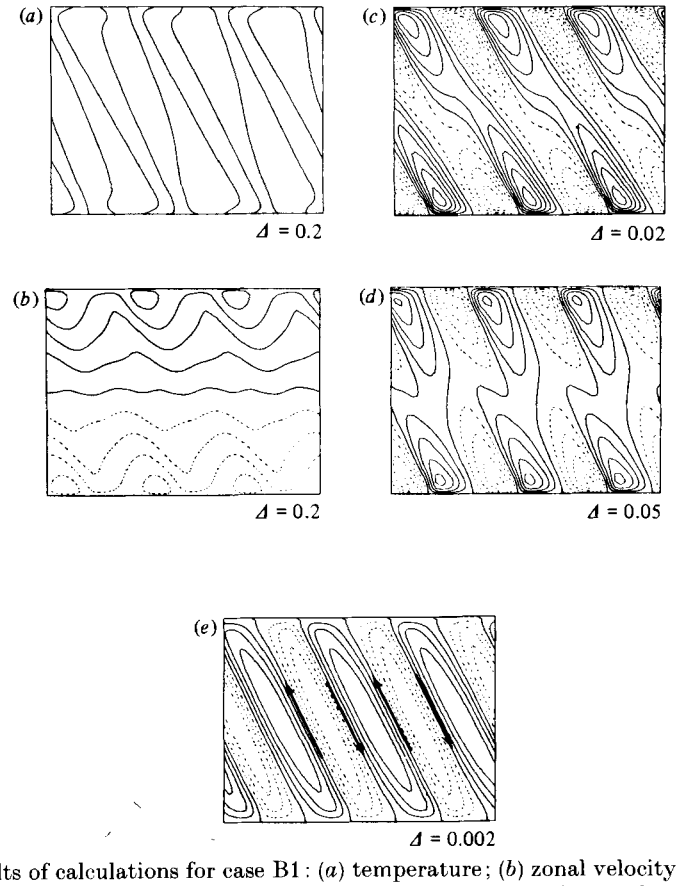

FIGURE 7. Results of calculations for case B1 : (*a*) temperature; (*b*) zonal velocity; (*c*) deviation T; (*d*) deviation u; (*e*) total ψ. Contour scheme is as in figure 3. See table 2 for true length/height aspect ratio.

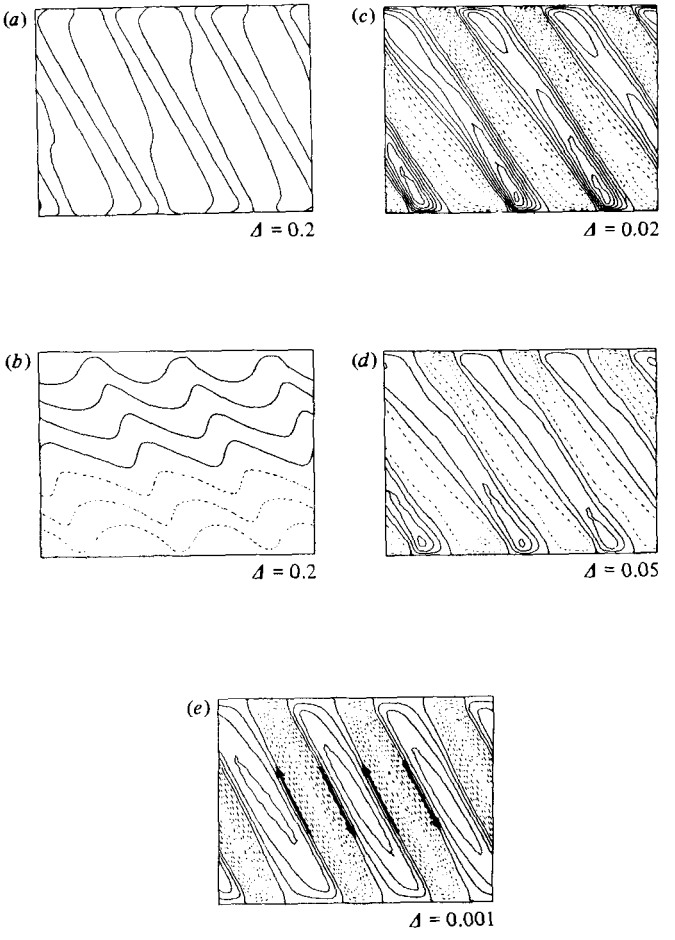

FIGURE 8. Results of calculations for case B2: (*a*) temperature; (*b*) zonal velocity; (*c*) deviation T; (*d*) deviation u; (*e*) total ψ. Contour scheme is as in figure 3. See table 2 for true length/height aspect ratio.

convection can occur. The study of these highly nonlinear flows is not pursued in this paper, other than to report some cases where they occurred (table 2).

The fields for case B2 ($Pr = 2$) are shown in figure 8. The relatively larger damping by viscosity of the inertial restoring force than of the buoyancy force by thermal diffusion results in the clockwise (CW) cells being of greater strength than the counterclockwise (CCW) cells. This is because advection by the CW cells tends to decrease the convective stability but to increase the inertial stability, and that CCW cells tend to do the opposite. When $Pr = 1$ these effects approximately cancel so that the cells are of similar strength. But when the inertial restoring force is suppressed, the advection of heat by the cells acts to destabilize the CW cells and to stabilize the CCW cells, without compensation by the advection of momentum. (For $Pr < 1$ (case B3) the inertial force is dominant, and the opposite is true (figure 9).) Furthermore, in the case of $Pr > 1$, the advection of angular momentum is dominated by the Coriolis term, and the inertial stability is actually greater in the vicinity of the CW cells, contrary to the effects of nonlinear advection. For $Pr < 1$ (case B3), on the other hand, the zonal velocity field is in response to the nonlinear advection by the cells. This point is illustrated by figure 10, where the total zonal velocity fields

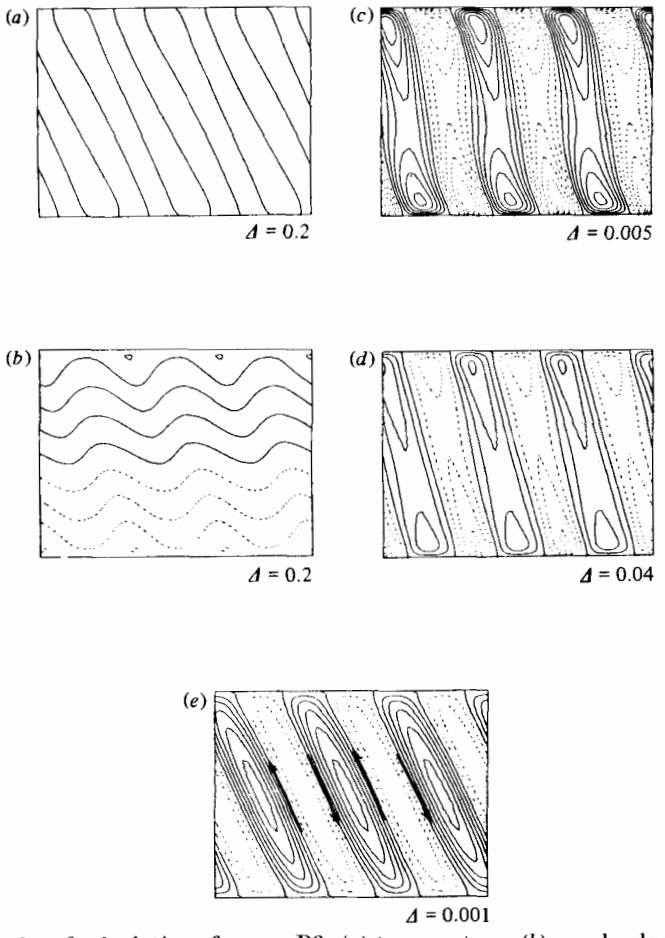

FIGURE 9. Results of calculations for case B3: (*a*) temperature; (*b*) zonal velocity; (*c*) deviation T; (*d*) deviation u; (*e*) total ψ. Contour scheme is as in figure 3. See table 2 for true length/height aspect ratio.

are overlayed with the stream-function fields. A similar effect occurs with the thermal advection. Nonlinear advection is important for $Pr = 2$ but not for $Pr = 0.5$, where advection of the basic horizontal gradient dominates. An effect of Pr and nonlinearity is seen in the flow out of the boundary layer. That clockwise cells are stronger for $Pr = 2$ results in the upward motion out of the lower boundary layer bringing relatively warm fluid upward and in cold fluid being brought downward out of the upper boundary layer. That counterclockwise cells are stronger for $Pr = 0.5$ results in the transport of cold fluid upward out of the lower boundary layer, and in the transport of warm fluid downward from the upper boundary layer. After leaving the boundary layer, the thermal deviation is retained for $Pr = 2$ but not for $Pr = 0.5$.

Table 3 gives the energy-conversion integrals and energy changes from the analytic basic state to that with waves for some of the cases computed. The quantities $\langle \overline{\mathrm{KE}} \rangle$, $\langle \mathrm{KE}' \rangle$ and $\langle \mathrm{PE} \rangle$ are normalized by dividing by the analytic basic state $\langle \mathrm{KE} \rangle$. The energy-conversion integrals were normalized by $\langle \mathrm{KE}' \rangle$. The effect of Prandtl number upon the energetics of the flow is quite strong. A schematic diagram of the energy transfer for cases B1, B2 and B3 is given in figure 11. The ultimate source for the

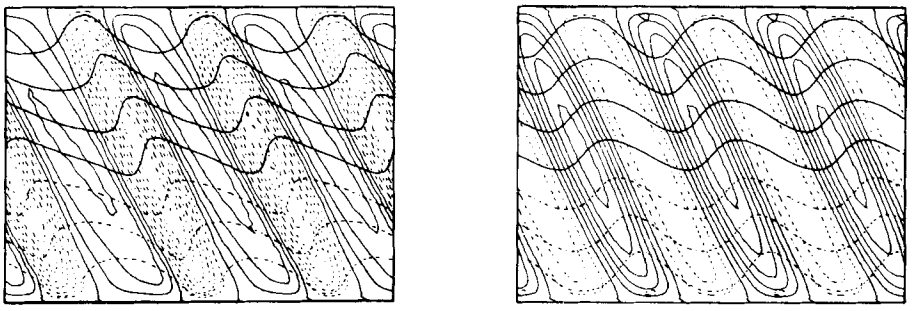

(a) (b)

FIGURE 10. Overlay of stream function and zonal velocity for cases B2 (*a*) and B3 (*b*).

wave KE′ in all cases is PE. For $Pr = 1$ and 2 the wave-energy source is $\langle E_1 \rangle$; for $Pr = 0.5$ the source is $\langle E_4 \rangle$ via $\langle E_2 \rangle$. Thus for $Pr = 0.5$ there is a thermally direct Hadley circulation induced by the waves which extracts PE. For $Pr = 2$ the induced circulation is in the opposite direction, thermally indirect, and is raising $\langle \mathrm{PE} \rangle$, although $\langle E_1 \rangle$ is large enough that the net effect of the waves upon $\langle \mathrm{PE} \rangle$ is that $\langle \mathrm{PE} \rangle$ is lowered. We note that for $Pr = 2$ the total change in $\langle \mathrm{PE} \rangle$ is relatively large. In all cases, $\langle \mathrm{PE} \rangle$ was decreased and $\langle \overline{\mathrm{KE}} \rangle$ was slightly increased as a result of the wave action. This is a result of the approximate equality of $\langle E_4 \rangle$ to $\langle E_2 \rangle$, rather than to $-\langle E_1 \rangle$.

That the effect of $\langle E_4 \rangle$ will tend to compensate for the effect of $\langle E_2 \rangle$, at least for small viscosity, may be seen from considering (2.17). Assuming $\langle E_3 \rangle$ is small (justified *a posteriori*)

$$\langle E_4 \rangle - \langle E_2 \rangle + \langle F \rangle \approx 0. \tag{3.1}$$

Note that $\langle E_4 \rangle = \langle \bar{v}z \rangle = \langle 2\bar{v}U \rangle$; i.e. that it is just the horizontal flux of basic-state angular momentum by the induced Hadley circulation. In the inviscid case this flux is balanced by the vertical eddy flux represented by $\langle E_2 \rangle$. Furthermore, if the zonal momentum equation (2.1) is multiplied by U and integrated

$$\langle E_4 \rangle + Ro\left\langle u'w'\frac{\partial U}{\partial z}\right\rangle + E\left\langle U\frac{\partial^2 \bar{u}}{\partial z^2}\right\rangle = 0. \tag{3.2}$$

Thus, in the inviscid case, any difference between $\langle E_4 \rangle$ and $\langle E_2 \rangle$ that would cause a decrease in $\partial\bar{u}/\partial z$ results in $\langle E_4 \rangle > \langle E_2 \rangle$, which is a contradiction since a decrease in $\partial\bar{u}/\partial z$ would occur only when $\langle E_2 \rangle > \langle E_4 \rangle$. A similar argunent can be made against any increase in $\partial\bar{u}/\partial z$. In the viscous case, a significant difference between $\langle E_2 \rangle$ and $\langle E_4 \rangle$ can be tolerated, since viscous diffusion can dissipate the excess momentum flux. This difference was small in all cases computed here except for case B7. It is interesting that in all cases $\langle E_4 \rangle$ was very much closer to $\langle E_2 \rangle$ than to $-\langle E_1 \rangle$, in view of the inviscid forms of (2.15) and (3.1), in which all three must be equal. That is, diffusion apparently totally releases the constraint that $\langle E_4 \rangle = -\langle E_1 \rangle$, but does not *greatly* release the constraint that $\langle E_4 \rangle \approx \langle E_2 \rangle$. Thus the average potential energy is much more affected by the waves than the average kinetic energy. Note that, for the opposite to be true, $\langle \bar{F} \rangle$ would have to be positive and of equal magnitude to $\langle F' \rangle$. Although this is not a *priori* an impossibility, it was never observed here. Note that the result of the nonlinear work of Walton (1975) was that $\langle E_4 \rangle \equiv \langle E_2 \rangle$. This is because he assumed small nonlinear effects and neglected friction when solving the second-order momentum equations. He did not neglect thermal diffusion in the

Case	$\langle KE' \rangle$	$\langle \Delta\overline{KE} \rangle$	$\langle \Delta PE \rangle$	$\langle E_1 \rangle$	$\langle E_2 \rangle$	$\langle E_3 \rangle$	$\langle E_4 \rangle$	$\langle F \rangle$	$\langle F' \rangle$
B1	0.0572	0.0113	−0.333	0.543	0.0933	−0.00101	0.147	−0.690	−0.635
B2	0.0289	0.00597	−0.333	1.263	−0.627	0.00155	−0.577	−0.686	−0.637
B3	0.0269	0.00298	−0.160	−0.158	0.629	−0.00118	0.657	−0.499	−0.470
B6	0.0428	0.00164	−0.0595	0.114	0.995	−0.00909	1.073	−1.187	−1.100
B7	0.0255	0.0155	−0.148	0.468	0.221	−0.00402	0.397	−0.865	−0.685
B8	0.0378	0.00203	−0.0742	0.716	0.807	−0.00622	0.890	−1.606	−1.529

TABLE 3. Energetics

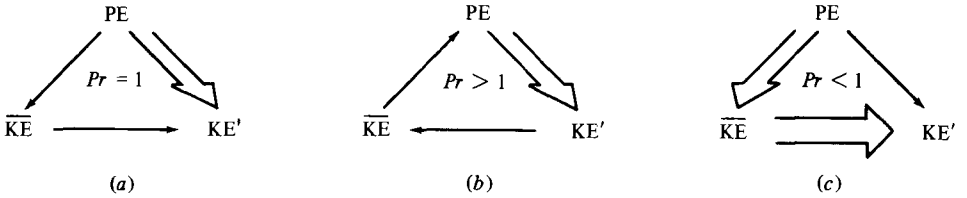

FIGURE 11. Schematic diagram of energy flow for cases B1, B2 and B3. Other $Pr = 1$ cases gave somewhat different results.

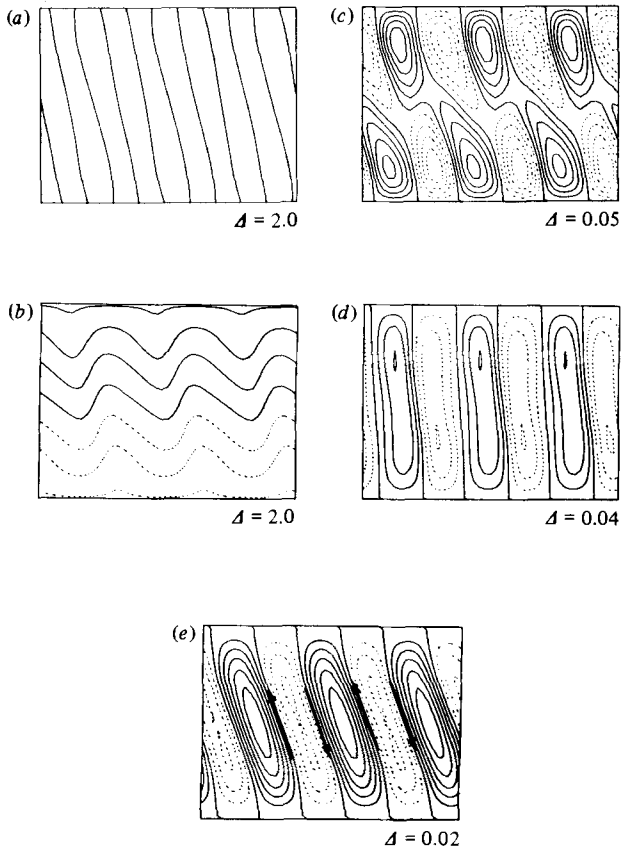

FIGURE 12. Results of calculations for case B6: (*a*) temperature; (*b*) zonal velocity; (*c*) deviation T; (*d*) deviation u; (*e*) total ψ. Contour scheme is as in figure 3. See table 2 for true length/height aspect ratio.

solution for the second-order temperature field, and therefore his $\langle E_1 \rangle$ and $\langle E_4 \rangle$ are not of equal magnitude. Thus the present results are not unexpected.

If the hydrostatic approximation is made, the dependence upon the thermal Rossby number is removed from the equations (Stone 1971; Walton 1975; Emanuel 1979). This approximation is valid when the parameter $S = Ri\,Ro^2$ ($= N^2/\Omega^2$, where N is the buoyancy frequency) is large. In general, however, there does exist a dependence upon the thermal Rossby number, as seen in the results of Weber (1980). For larger thermal Rossby number the critical Richardson number is increased; that is, the flow is more unstable. The present calculations confirmed this result: if all parameters (including Ri) are fixed at the same values as those for case B1 except that Ro is increased, the instabilities are more vigorous (case B9).

The energetics are also functions of Ro. For flows of large S (cases B6 and B7) the energy transformation $\langle E_2 \rangle$ becomes more important (this is consistent with the calculations by Emanuel 1979). Cases B6 and B7 are similar except that B6 is with much higher Ekman number, and may be compared with the no-slip cases of Emanuel. Although $\langle E_1 \rangle$ is not negative, as in Emanuel's cases, it is small compared with $\langle E_2 \rangle$, and thus the energy source may be considered to be inertial. The fields for case B6 are shown in figure 12. That $\langle E_2 \rangle$ becomes so important for the viscous hydrostatic case is due to the relatively large static stability, which gives preference to motions that are more nearly parallel to the isotherms (i.e. more vertical). When that is the case, the angular-momentum transport is greater than the heat transport (refer to figure 1). For a non-hydrostatic case with larger Ekman numbers (B8), $\langle E_1 \rangle$ and $\langle E_2 \rangle$ are both positive, and are in fact almost equal.

4. Summary

Fully developed, quasi-steady symmetric baroclinic waves have been computed for two configurations, both of which have temperature profiles with constant horizontal gradients imposed upon upper and lower boundaries. The horizontal length of the physical domain has been assumed to be large compared with the vertical. The first configuration was that with corotating upper and lower boundaries, resulting in thermally direct boundary-layer flow (i.e. Hadley cell) in the basic state. The second configuration was that with the upper and lower boundaries moving with the zonal wind such that there were no boundary layers in the basic state. Both configurations were of no-slip horizontal boundaries.

Calculations showed that the thermal boundary layers in the first (Hadley-cell) configuration may be convectively unstable. When this was the case, a steady flow could not be found, and symmetric baroclinic waves were not well defined. Therefore, detailed study of symmetric baroclinic instability (SBI) was given to the second configuration.

Cases were computed with independently varied Ro, Ri, E and Pr. The waves are stronger for smaller Ri and E, for larger Ro, and for Pr away from one. The region in parameter space where the waves are weak enough to result in steady flow is not large; as any of the parameters are varied to give stronger waves there is indication that turbulence can arise due perhaps to strong horizontal shear in the waves, to regions of negative vertical temperature derivative, or to both. A propensity for the waves to result in strong fronts was noted. More detailed calculations are required to study these aspects of SBI.

In all cases, the energy source for the waves was the flow's potential energy and the basic state zonal flow was insignificantly affected by the waves. For $Pr < 1$ the

energy conversion was from potential energy to mean kinetic energy to wave kinetic energy. For $Pr > 1$ the energy conversion was directly from potential energy to wave kinetic energy. For $Pr = 1$ the energy conversion was by either or both methods, depending upon the other parameters. The effect upon the mean flow was to slightly raise the mean kinetic energy, primarily the result of a mean meridional flow. The induced mean meridional circulation was thermally direct for $Pr < 1$ and thermally indirect for (large enough) $Pr > 1$, such as to approximately cancel the effect of vertical eddy flux of angular momentum.

The results here suggest that a search for symmetric baroclinic instability in the laboratory can best be performed by either using a low-Prandtl-number fluid or by an annulus with differentially rotating top and bottom. Otherwise, thermal convection in the boundary layers may prevent the development of SBI, although it may be possible to avoid this complication by not allowing Ro to become too large.

Since the model utilized here allows no longitudinal variations, the flows calculated may or may not be seen in a real situation which is approximated by the current idealized configurations. The basic state and/or the fully developed SBI flows may be unstable to perturbations with longitudinal variations. Busse & Chen (1981) have suggested that the maximum linear growth rate is not achieved for purely symmetric waves. Antar & Fowlis (1983) have shown that, for small enough Ri, the maximum growth rate is in fact achieved when very long wavelengths in the longitudinal direction are allowed. Thus, the flows here may be expected to be close to those that would be observed in an experiment whose geometry is well approximated by the infinite channel.

The results of the present study showing that vigorous two-dimensional waves are possible have interesting implications for works which attempt to determine regime diagrams numerically by first calculating a two-dimensional flow and then testing the stability of that flow to three-dimensional perturbations. The study by Miller & Gall (1983*b*), for example, was successful in using this technique to calculate the transition curve for the baroclinic annulus. This technique may not work, however, if there exist both two-dimensional and three-dimensional instabilities which may in reality be competing for the same energy source (in this case, potential energy). A calculation of the two-dimensional basic state may allow the two-dimensional modes to 'consume' the energy first, without competition. Such a case may result in a prediction of two-dimensional flow where in the real situation three-dimensional disturbances are observed. In the ideal situation studied here, where an analytic basic state is known, a strictly linear approach (e.g. Antar & Fowlis 1983) would perhaps be more valid in determining the most likely disturbance to be seen. Nonlinear models would be required, of course, to determine whether the different disturbances can coexist, or whether a (linearly) slower growing disturbance can eventually overtake the faster growing one – perhaps resulting in the disappearance of the latter. In actual laboratory conditions, where an analytic basic state is not known, it may be necessary to use a two-dimensional model that can find the multiple steady states, or to use a fully nonlinear three-dimensional model in order to determine quantitatively a transition curve. The results of the latter technique may be sensitive to initial conditions.

Most of this work was performed while the author was a National Research Council postdoctoral associate at MSFC. He wishes to express gratitude for the support and encouragement from Dr W. W. Fowlis, his NRC adviser. The NRC associateship was funded by NASA, Office of Space Science and Applications, Atmospheric Processes Program.

REFERENCES

Antar, B. N. & Fowlis, W. W. 1982 Symmetric baroclinic instability of a Hadley cell. *J. Atmos. Sci.* **39**, 1280–1289.

Antar, B. N. & Fowlis, W. W. 1983 Three-dimensional baroclinic instability of a Hadley cell for small Richardson number. *J. Fluid Mech.* **137**, 425–447.

Bennetts, D. A. & Hoskins, B. J. 1979 Conditional symmetric instability as a possible explanation for frontal rainbands. *Q. J. R. Met. Soc.* **105**, 945–962.

Busse, F. H. & Chen, W. L. 1981 On the (nearly) symmetric instability. *J. Atmos. Sci.* **38**, 877–880.

Calman, J. 1977 Experiments on high Richardson number instability of a rotating stratified shear flow. *Dyn. Atmos. Oceans* **1**, 277–297.

Emanuel, K. A. 1979 Inertial instability and mesoscale convective systems. I. Linear theory of inertial instability in rotating viscous fluids. *J. Atmos. Sci.* **36**, 2425–2449.

Emanuel, K. A. 1982 Inertial instability and mesoscale convective systems. II. Symmetric CISK in a baroclinic flow. *J. Atmos. Sci.* **39**, 1080–1097.

Fowlis, W. W. & Hide, R. 1965 Thermal convection in a rotating annulus of liquid: effect of viscosity on the transition between axisymmetric and non-axisymmetric flow regimes. *J. Atmos. Sci.* **22**, 541–558.

Hadlock, R. K., Na, J. Y. & Stone, P. H. 1972 Direct thermal verification of symmetric baroclinic instability. *J. Atmos. Sci.* **29**, 1391–1393.

Hoskins, B. J. 1978 Baroclinic instability and frontogenesis. In *Rotating Fluids in Geophysics* (ed. P. H. Roberts & A. M. Soward). Academic.

McIntyre, M. E. 1970*a* Diffusive destabilization of the baroclinic circular vortex. *Geophys. Fluid Dyn.* **1**, 19–57.

McIntyre, M. E. 1970*b* Role of diffusive overturning in nonlinear axisymmetric convection in a differentially heated rotating annulus. *Geophys. Fluid Dyn.* **1**, 59–89.

Miller, T. L. & Gall, R. L. 1983*a* Thermally driven flow in a rotating spherical shell: axisymmetric states. *J. Atmos. Sci.* **40**, 856–868.

Miller, T. L. & Gall, R. L. 1983*b* A linear analysis of the transition curve for the baroclinic annulus. *J. Atmos. Sci.* **40**, 2293–2303.

Ooyama, K. 1966 On the stability of the baroclinic circular vortex: a sufficient criterion for instability. *J. Atmos. Sci.* **23**, 43–53.

Quon, C. 1980 Quasi-steady symmetric regimes of a rotating annulus differentially heated on the horizontal boundaries. *J. Atmos. Sci.* **37**, 2407–2423.

Quon, C. 1981 In search of symmetric baroclinic instability in an enclosed rotating fluid. *Geophys. Astrophys. Fluid Dyn.* **17**, 171–197.

Stone, P. H. 1966 On non-geostrophic baroclinic stability. *J. Atmos. Sci.* **23**, 390–400.

Stone, P. H. 1970 On non-geostrophic baroclinic stability: Part II. *J. Atmos. Sci.* **27**, 721–726.

Stone, P. H. 1971 Baroclinic stability under non-hydrostatic conditions. *J. Fluid Mech.* **45**, 659–671.

Stone, P. H. 1972 On non-geostrophic baroclinic stability: Part III. The momentum and heat transports. *J. Atmos. Sci.* **29**, 419–426.

Stone, P. H., Hess, S., Hadlock, R. & Ray, P. 1969 Preliminary results of experiments with symmetric baroclinic instability. *J. Atmos. Sci.* **26**, 991–996.

Tokioka, T. 1970 Non-geostrophic and non-hydrostatic stability of a baroclinic fluid. *J. Met. Soc. Japan* **48**, 503–520.

Walton, I. C. 1975 The viscous nonlinear symmetric baroclinic instability of a zonal shear flow. *J. Fluid Mech.* **68**, 757–768.

Weber, J. E. 1980 Symmetric instability of stratified geostrophic flow. *Tellus* **32**, 176–185.

Williams, G. P. 1968 Thermal convection in a rotating fluid annulus: Part 3. Suppression of the frictional constraint on lateral boundaries. *J. Atmos. Sci.* **25**, 1034–1045.

Williams, G. P. 1970 Axisymmetric annulus convection at unit Prandtl number. *Geophys. Fluid Dyn.* **1**, 357–369.

Yanai, M. & Tokioka, T. 1969 Axially symmetric meridional motions in the baroclinic circular vortex: a numerical experiment. *J. Met. Soc. Japan* **47**, 183–197.